Journal of Power Sources 267 (2014) 459–468

Contents lists available at ScienceDirect

Journal of Power Sources

journal homepage: www.elsevier.com/locate/jpowsour

Carbon nanotube-loaded mesoporous $LiFe_{0.6}Mn_{0.4}PO_4$/C microspheres as high performance cathodes for lithium-ion batteries

Yingying Mi, Ping Gao, Wen Liu*, Weidong Zhang, Henghui Zhou*

College of Chemistry and Molecular Engineering, Peking University, Beijing 100871, China

HIGHLIGHTS

- Mesoporous $LiFe_{0.6}Mn_{0.4}PO_4$/C with MWCNTs was synthesized by spray drying process.
- MWCNTs entangle with primary particles to form interconnected conducting network.
- MWCNTs loaded $LiFe_{0.6}Mn_{0.4}PO_4$/C exhibits ultra-high rate capability even at 50 C.
- The $LiFe_{0.6}Mn_{0.4}PO_4$/C microspheres behave very stable cycling performance at 45 °C.

ARTICLE INFO

Article history:
Received 28 January 2014
Received in revised form
20 May 2014
Accepted 21 May 2014
Available online 2 June 2014

Keywords:
Lithium ion battery
Lithium iron manganese phosphate
High performance
Multiwall carbon nanotube
Spray dry

ABSTRACT

A series of $LiFe_{0.6}Mn_{0.4}PO_4$/C composites with different amount of multiwall carbon nanotubes (MWCNTs) has been successfully synthesized by introducing MWCNTs to $LiFe_{0.6}Mn_{0.4}PO_4$ microspheres during the spray drying process. The as-prepared mesoporous spherical products (5–20 μm) are composed of primary nanoparticles (~100 nm) and open-mesopores distribute both on the surface and inside the microspheres. XRD patterns and HRTEM images indicate that the as-prepared $LiFe_{0.6}Mn_{0.4}PO_4$/C composites are well crystallized and no impurity phase is observed. As MWCNTs can entangle with the primary particles to form an interconnected conducting network, which can facilitate the electron transference, their existence can greatly enhance the conductivity between particles. Therefore, they can obviously increase the rate capability especially working at high current densities. Among the $LiFe_{0.6}Mn_{0.4}PO_4$/C micro-spherical samples, the composite with 2% MWCNTs loading shows the best electrochemical performance, delivering a capacity of 163.3 mAh g^{-1} at 0.1 C, which is almost 96% of the theoretical capacity (~170 mAh g^{-1}). When discharged at 50 C, the composite still exhibits obviously higher capacity (64.23 mAh g^{-1}) than the $LiFe_{0.6}Mn_{0.4}PO_4$/C without MWCNTs (12.8 mAh g^{-1}). Moreover, the MWCNTs embedded composite shows high cycle stability with no apparent capacity fading or voltage decay after 500 cycles at 45 °C.

1. Introduction

As one of the most promising candidate cathode materials for lithium ion batteries (LIBs), olivine-structural $LiFePO_4$ has attracted wide attention and been widely studied since 1997 [1], due to its relatively high theoretical capacity (~170 mAh g^{-1}), high safety, and low cost. Nevertheless, some intrinsic drawbacks greatly limit its application in transportation and grid energy storage, such as low conductivity, low energy density, and poor process ability for electrode [2,3]. To overcome its conductive problem, many methods have been reported such as size reduction to nanoscale levels [4–6], conductive materials coating [7–10] and supervalent cations doping [11–13]. To further increase energy density, many researchers turn to the iso-structural $LiMnPO_4$ because of its higher operating voltage (4.1 V vs. Li/Li^+) and larger theoretical energy density (684 W h kg^{-1}) than that of $LiFePO_4$ respectively (3.4 V vs. Li/Li^+; 586 W h kg^{-1}) [14,15]. However, the electronic conductivity of $LiMnPO_4$ (<10^{-10} S cm^{-1}) is even lower than that of $LiFePO_4$ (~10^{-8} S cm^{-1}), resulting in its poorer rate capability [16]. As such, it was proposed that the coexistence of the $LiMnPO_4$ and $LiFePO_4$ [17,18] or partial substitution of Fe^{2+} for Mn^{2+} in $LiMnPO_4$ may improve the electrode kinetics during the charge–discharge process, leading to better electrochemical performance [19].

* Corresponding authors. Tel./fax: +86 10 62757908.
E-mail addresses: liuwen-03721@163.com (W. Liu), hhzhou@pku.edu.cn (H. Zhou).

http://dx.doi.org/10.1016/j.jpowsour.2014.05.102
0378-7753/

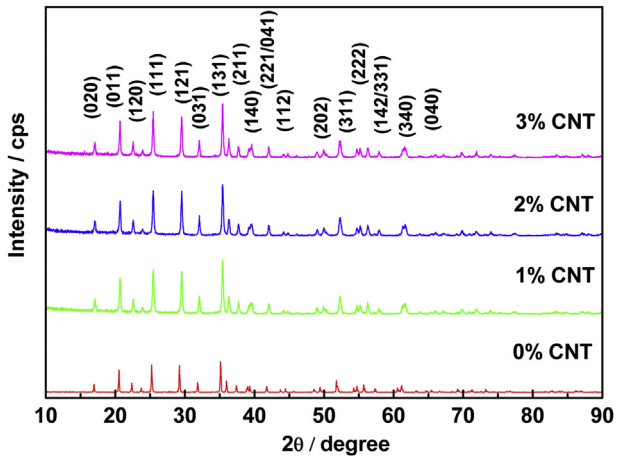

Fig. 1. XRD patterns of mesoporous $LiFe_{0.6}Mn_{0.4}PO_4$/C microspheres with different MWCNTs content (0%, 1%, 2% and 3%).

Recently, major attention has been devoted to $LiFe_xMn_{1-x}PO_4$, intending to improve the electrochemical properties while maintaining relative high energy density [20–26]. Among all these methods explored, carbon coating is a common and effective way to overcome the limitation of low electronic conductivity as the well dispersed carbon can provide pathways for electron transference [27]. However, most of the coated carbon layers exhibit an sp3 structure rather than sp2 graphene structure. It is believed that sp3 carbon is inferior to graphene in improving conductivity of electrode materials. Moreover, carbon modification of the particle's surface can only facilitate electron distribution among particles through a "point to point" mode, while the improvement of conductivity between particles which mainly depends on the effective transference of electrons in the interconnected network is much limited [28,29].

As advanced one-dimensional carbon materials with sp2 structure, MWCNTs can be used as additives in the electrode due to their properties of short diffusion path for electron transport, large surface area and fast electronic/thermal conductions [30,31]. The electronic conductivity of MWCNTs is about $(1–4) \times 10^2$ S cm^{-1} along the nanotube axis and 5–25 S cm^{-1} perpendicular to the axis [27]. MWCNTs can entangle with particles to form interconnected network, which is easier for electrons to distribute and transport between particles. There are some literatures reported about $LiFePO_4$/MWCNT composite materials. The ways to introduce MWCNTs to the host materials include hydrothermal route [27,32], microwave heating [33], and mixing MWCNTs directly when fabricating electrodes [34]. These methods mentioned above are not convenient for scale up, nor deficient in effect function as conductive lead to connect particles and facilitate fast charge transfer to improve rate capability at high current. Furthermore, few researchers discussed about the influence of MWCNTs loading

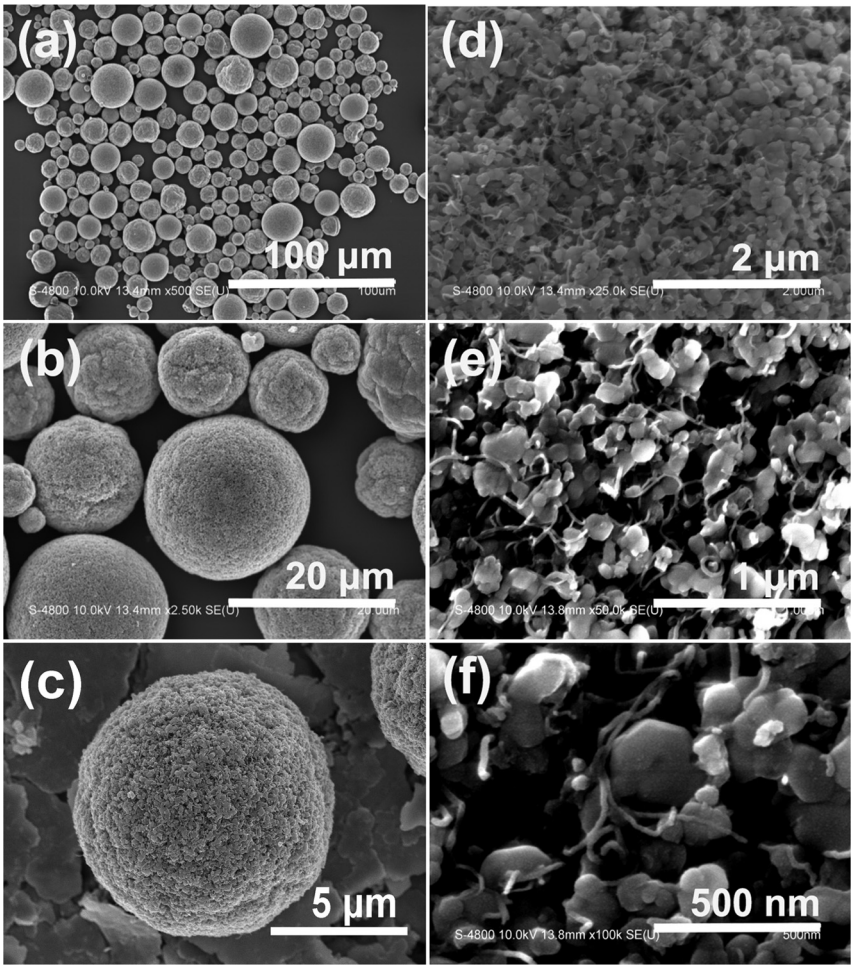

Fig. 2. SEM images of mesoporous $LiFe_{0.6}Mn_{0.4}PO_4$/C microspheres with 2% MWCNTs content.

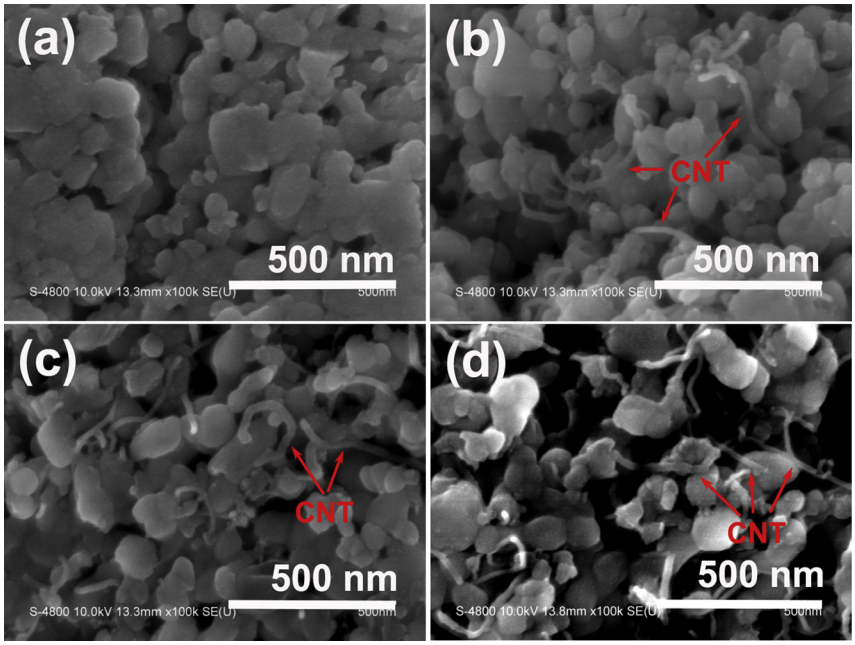

Fig. 3. FESEM images of mesoporous $LiFe_{0.6}Mn_{0.4}PO_4/C$ microspheres with different MWCNTs content: (a) 0%, (b) 1%, (c) 2%, (d) 3%.

on the stability at relatively high rates under high temperature and with prolonged cycles.

In this work, we synthesized a series of $LiFe_{0.6}Mn_{0.4}PO_4/C$ composites with different MWCNTs amount by taking advantage of the spray drying method, which is a facile and scalable technique to fabricate micro-sized spherical materials [16]. Mesopores distributed uniformly both on the surface and in the microspheres. The porous strategy allows efficient percolation of electrolyte through the electrode, favoring the Li^+ access to active material via the mesopores, contributing to efficient use of electrode materials. What's more, MWCNTs were also introduced to microspheres during the process of spray drying, which entangled with the primary particles to form conducting network that can facilitate the electron transference between particles, leading to exceptional electrochemical performance of $LiFe_{0.6}Mn_{0.4}PO_4/C$ composite. Ultra-high rate capability of 64.23 mAh g^{-1} at 50 C can be achieved with 2% MWCNTs loading, comparing to 12.8 mAh g^{-1} of bare sample without MWCNTs. The electrochemical results demonstrate that the MWCNTs loaded $LiFe_{0.6}Mn_{0.4}PO_4/C$ microspheres can exhibit both high rate capability and high stability, which make them very attractive as cathode materials for next generation lithium-ion batteries used in electric vehicles and grid energy storage.

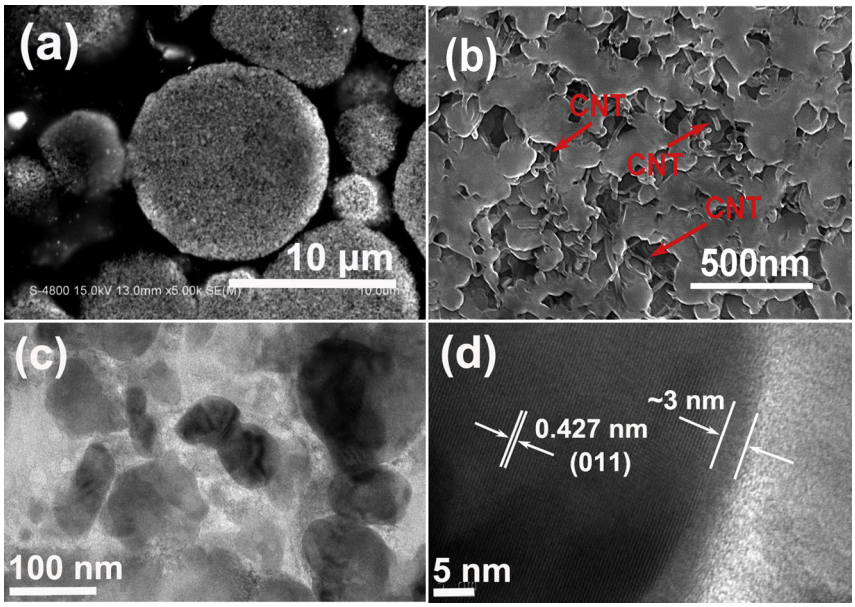

Fig. 4. Cross-sectional SEM image (a) and magnified cross-sectional SEM image (b) of a single $LiFe_{0.6}Mn_{0.4}PO_4/C$ microsphere with 2% MWCNTs content; magnified cross-sectional TEM image (c) and HRTEM image (d) of a single $LiFe_{0.6}Mn_{0.4}PO_4/C$ microsphere with 2% MWCNTs content.

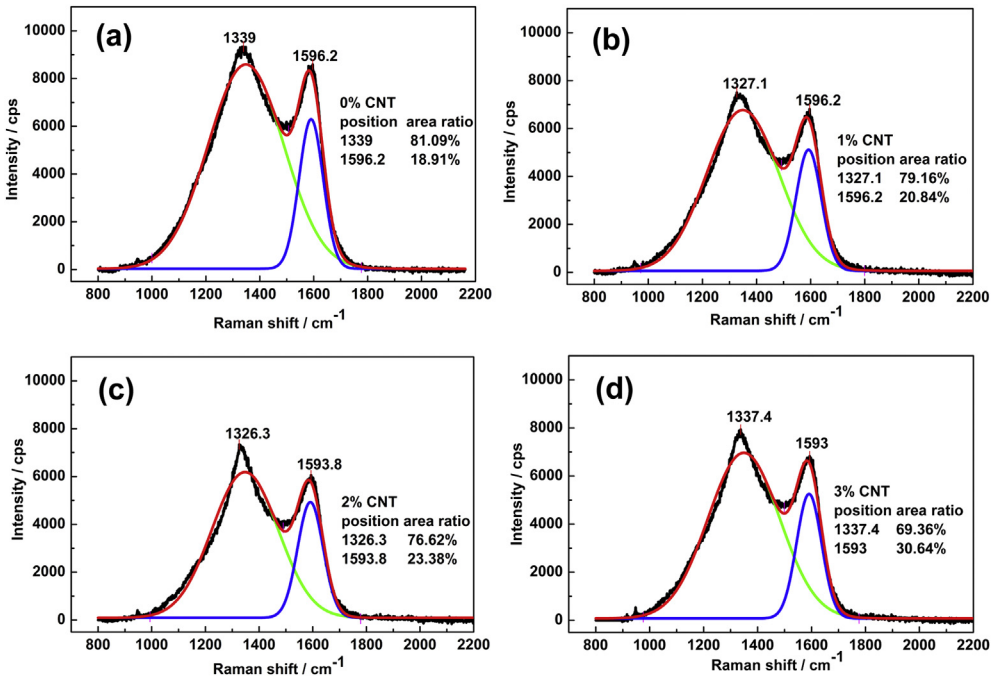

Fig. 5. Raman spectroscopy of mesoporous $LiFe_{0.6}Mn_{0.4}PO_4$/C microspheres with different MWCNTs content: (a) 0%, (b) 1%, (c) 2%, (d) 3%.

2. Experimental

2.1. Preparation of materials

Firstly, $(Fe_{0.6}Mn_{0.4})C_2O_4 \cdot 2H_2O$ was prepared according to reference [16]. The specific steps are as follows. Under protection of N_2 atmosphere, 0.5 M ammonium oxalate solution was pumped to 0.5 M transition metal sulphate solution in the tank reactor to form a bright yellow precipitate immediately. After washed several times with distilled water, the precipitate was then dried in a vacuum oven at 80 °C for 10 h.

Preparation of $LiFe_{0.6}Mn_{0.4}PO_4$/C composite involved a two-step carbon coating and spray drying process. In the first carbon coating process, stoichiometric amounts of as-prepared $(Fe_{0.6}Mn_{0.4})C_2O_4 \cdot 2H_2O$, Li_2CO_3 (AR, Shanghai Chemical Agents Co. Ltd), $NH_4H_2PO_4$ (AR, Shanghai Chemical Agents Co. Ltd) and sucrose (10% molar ratio, AR, Shanghai Chemical Agents Co. Ltd) were dispersed in ethanol (AR, Sinopharm Chemical Reagent Beijing Co. Ltd) and then

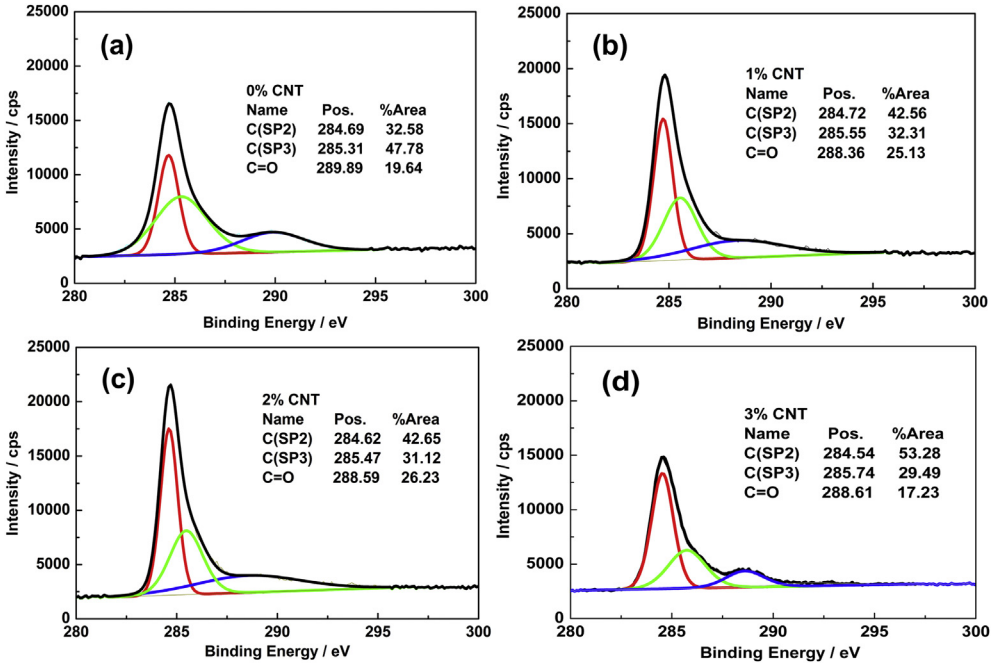

Fig. 6. XPS of mesoporous $LiFe_{0.6}Mn_{0.4}PO_4$/C microspheres with different MWCNTs content: (a) 0%, (b) 1%, (c) 2%, (d) 3%.

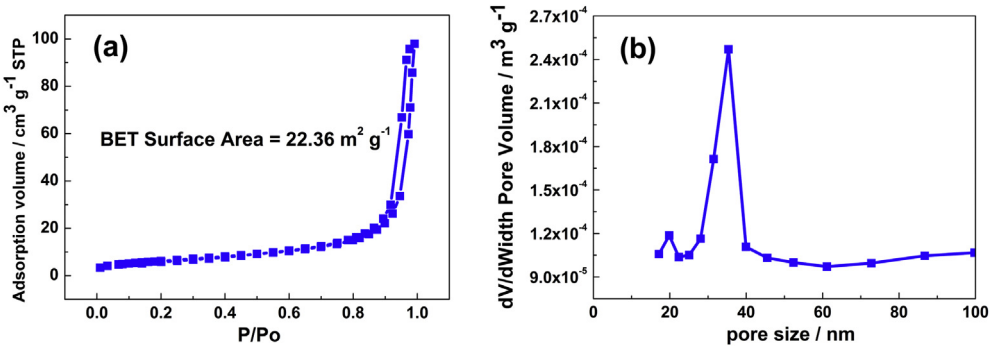

Fig. 7. N_2 adsorption–desorption isotherm (a) and BJH pore size distribution (b) of the $LiFe_{0.6}Mn_{0.4}PO_4$/C microspheres.

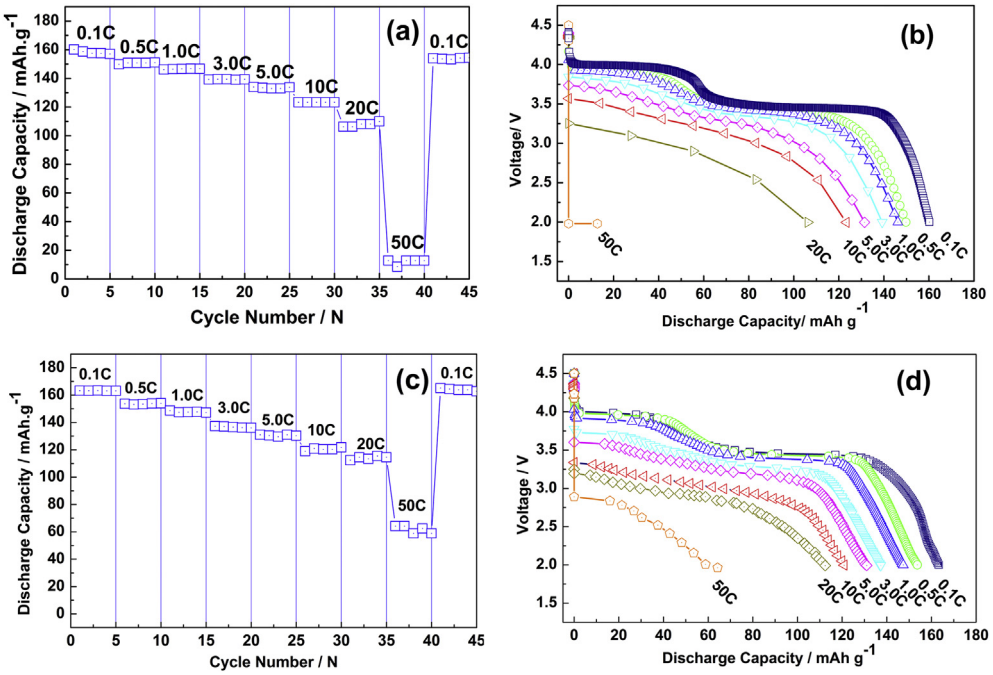

Fig. 8. Rate capability of the $LiFe_{0.6}Mn_{0.4}PO_4$/C microspheres without MWCNTs under different rates (a) and the corresponding discharge curves (b); rate capability of the $LiFe_{0.6}Mn_{0.4}PO_4$/C microspheres with 2% MWCNTs content under different rates (c) and the corresponding discharge curves (d).

ball-milled for 3 h. In order to get a uniform carbon coating layer, the mixture was dried for 2 h under vacuum at 100 °C and then transferred to a tube furnace, heating at 550 °C for 3 h under N_2 atmosphere.

After then, the second carbon coating process was carried out. The mixture of pre-sintered product (carbon content of about 1 wt %), PEG400 (as a dispersant), sucrose, and MWCNTs was ball-milled in deionized water for 5 h to make a slurry. During the ball-milling process, the adding amounts of sucrose and MWCNTs were adjusted to control the carbon content of the final products to about 3.5 wt%. In the spray drying setup, the feeding slurry was pumped to the centrifugal atomizer and sprayed into aerosol, and then spherical powders formed since the moisture evaporated quickly with the heated air flowing. Finally, the spray dried products were annealed at 650 °C for 10 h with N_2 flowing, and named as "$LiFe_{0.6}Mn_{0.4}PO_4$/C microspheres". For comparison, the $LiFe_{0.6}Mn_{0.4}PO_4$/C microspheres without MWCNTs were also fabricated via the similar method except that MWCNTs were absent during the subsequent carbon coating process.

2.2. Characterization

The crystal structures of all samples were characterized through X-ray diffraction (XRD, D/max2500PC, Rigaku) using Cu Kα radiation ($V = 40$ kV, $I = 100$ mA). The scanning range was from 10 to 90° at a scan rate of 4° min^{-1}. Carbon property analysis was carried out utilizing Raman spectroscopy (LabRam JY HR800) and X-ray Photoelectron Spectroscopy (XPS, Kratos Analytical Ltd). The morphologies of the as-prepared $LiFe_{0.6}Mn_{0.4}PO_4$/C composites were investigated through Scanning Electron Microscopy (SEM, S4800, Hitachi). Analysis of the elemental distribution of the particles was performed using a SEM based energy-dispersive X-ray (EDX) spectroscopic detector (INCA, Oxford, UK). The microstructures and carbon coating layers of the particles were observed by High Resolution Transmission Electron Microscopy (HRTEM, Tecnai G2). Nitrogen adsorption isotherm was measured at 77 K after degassing of the sample at 150 °C for more than 2 h (ASAP2020, Micromeritics, USA).

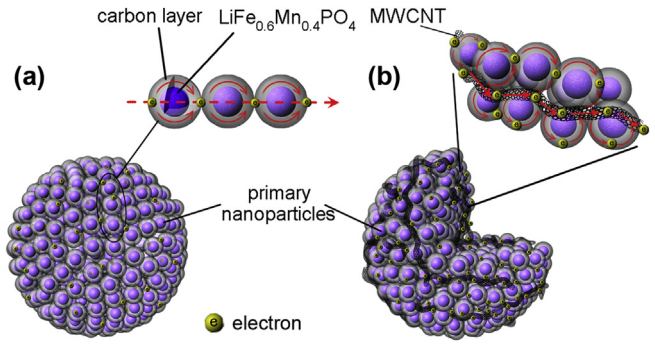

Fig. 9. The schematic representation of $LiFe_{0.6}Mn_{0.4}PO_4$/C microspheres without MWCNTs (a) and with MWCNTs (b).

2.3. Electrochemical performance

The electrochemical performance of the samples was evaluated using CR2032 coin-type cells. The cathode slurry was made by mixing active material, black carbon and polyvinylidene fluoride (PVDF) with a weight ratio of 8:1:1 in N-methyl pyrrolidinone and stirred for about 24 h. Then the slurry was pasted onto aluminum foil, and dried for 2 h at 90 °C. After that, the aluminum foil with active material was punched into 12 mm-diameter disks and dried in a vacuum oven at 120 °C for 24 h. The electrolyte used was 1 M $LiPF_6$ dissolved in a mixed solvent of ethylene carbonate (EC)–dimethyl carbonate (DMC)–ethyl methyl carbonate (EMC) (1:1:1 volume ratio, LB315 produced by Zhangjiagang Guotai-Huarong New Chemical Materials Co., Ltd). The separator was a polypropylene membrane (Celgard 2400). Lithium metal served as both a counter and reference electrode.

At last, the cells were assembled in a glove box with dry Argon atmosphere (Master 100 Lab, Braun, Germany) and tested by a battery testing system at voltages ranging from 2 V to 4.5 V at different current densities (LAND CT2001A, Wuhan Kinguo Electronics Co., Ltd). The cyclic voltammetry (CV) tests were carried out on an electrochemical workstation (CHI660D, CH Instruments) in a voltage range of 2.0–4.5 V. Electrochemical Impedance Spectroscopy (EIS) was also measured on the electrochemical workstation over a frequency range of 100,000 Hz–0.01 Hz.

3. Results and discussion

The crystallinity of mesoporous $LiFe_{0.6}Mn_{0.4}PO_4$/C microspheres with different MWCNTs content is shown in Fig. 1. All of the diffraction peaks are perfectly coherent with the standard PDF card (#33-0804), and no impurity phase is detected, which indicates an integrated olivine structure. The sharp peak shape indicates that the as-synthesized composites are well crystallized. In the XRD patterns, no peak can be associated with MWCNTs owing to the small amount of MWCNTs added.

Fig. 2 is SEM images of mesoporous $LiFe_{0.6}Mn_{0.4}PO_4$/C microspheres with 2% MWCNTs content in different magnification. The introduction of MWCNTs cannot change the spherical morphology of the spray dried particles. From the images, we can find that the $LiFe_{0.6}Mn_{0.4}PO_4$/C microspheres with 2% MWCNTs loading exhibit a secondary particle structure with size of about 5–20 μm, and the surface is made accessible with open-mesopores. The SEM images clearly show the uniform distribution of MWCNTs (Fig. 2). In the magnified images, MWCNTs entangling with the primary particles in the microspheres can be seen, which facilitates the construction of the interconnected conducting network. Moreover, FESEM images in Fig. 3 indicate that the introduction of the MWCNTs to $LiFe_{0.6}Mn_{0.4}PO_4$/C microspheres cannot change the size of the primary particles (~100 nm) and the mesoporous structure. What's more, with increasing adding amount, more MWCNTs can be observed on the surface of the microspheres. These MWCNTs entangle with the primary particles, forming interconnected conducting networks in the second microspheres. Therefore, electron transference in the electrode materials becomes even easier.

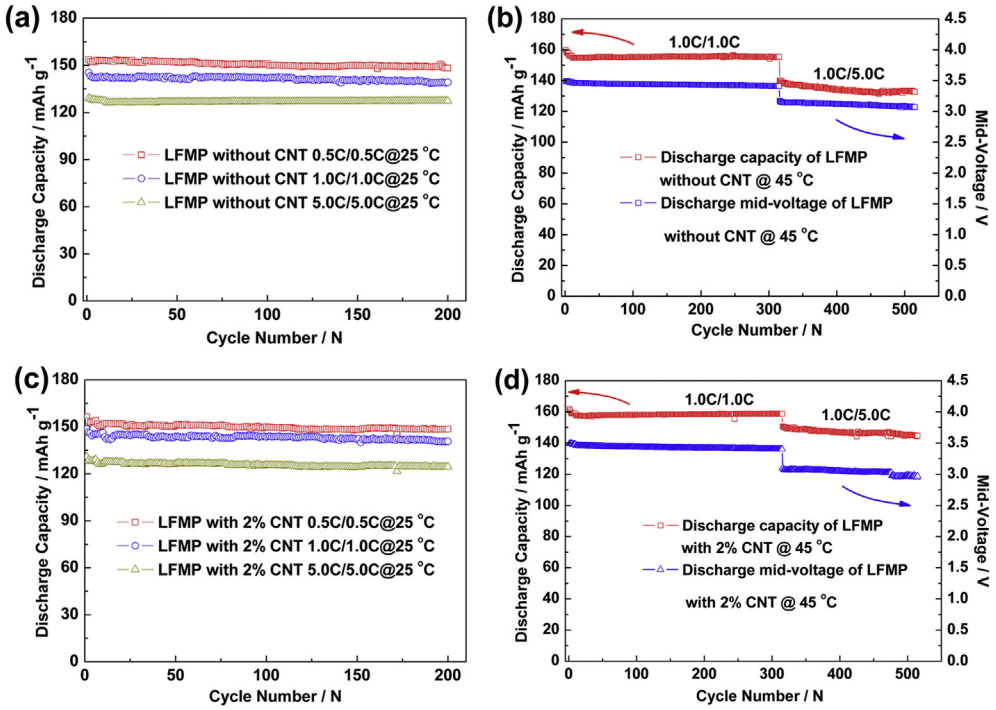

Fig. 10. Cycle performance of $LiFe_{0.6}Mn_{0.4}PO_4$/C microspheres without MWCNTs at 25 °C (a) and 45 °C (b); cycle performance of $LiFe_{0.6}Mn_{0.4}PO_4$/C microspheres with 2% MWCNTs content at 25 °C (c) and 45 °C (d).

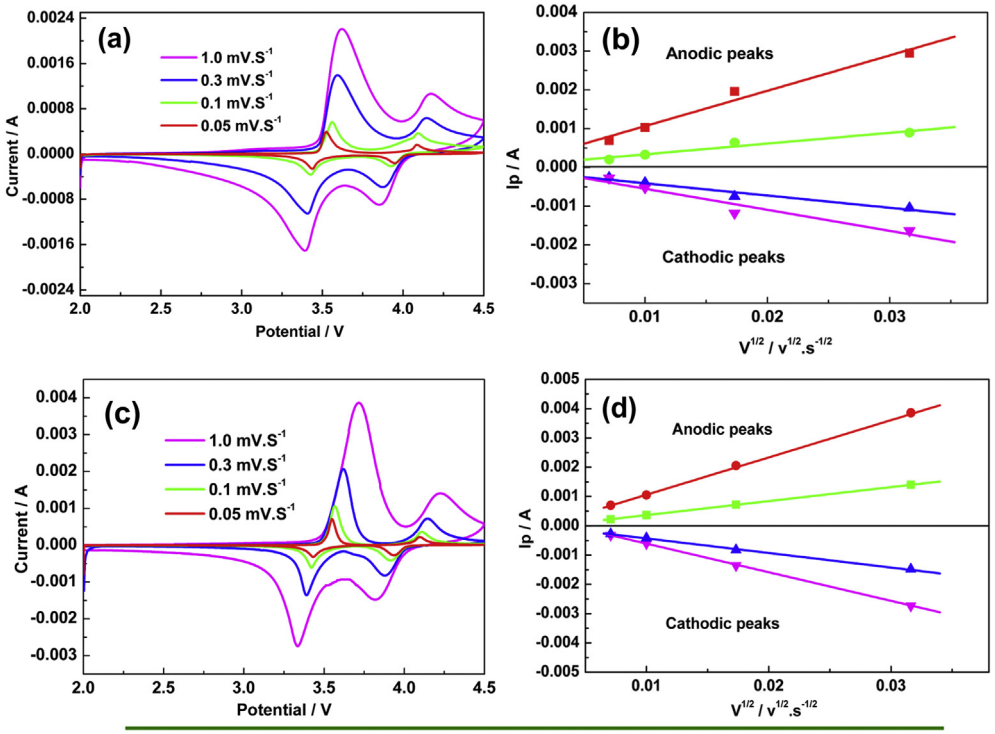

(e)

State	Peaks	Ds(cm².s⁻¹)	
		0%CNT	2%CNT
Charge	A_{Fe}	7.6E-12	8.9E-12
	A_{Mn}	5.6E-13	6.0E-13
Discharge	C_{Fe}	1.2E-12	5.2E-12
	C_{Mn}	4.5E-13	6.5E-13

Fig. 11. CV curves at different scan rates (a) and the linear relationship of I_p vs. $v^{1/2}$ (b) of $LiFe_{0.6}Mn_{0.4}PO_4$/C microspheres without MWCNTs; CV curves at different scan rates (c) and the linear relationship of I_p vs. $v^{1/2}$ (d) of $LiFe_{0.6}Mn_{0.4}PO_4$/C microspheres with 2% MWCNTs content; Li^+ diffusion coefficient Ds of the $LiFe_{0.6}Mn_{0.4}PO_4$/C microspheres without and with 2% MWCNTs (e).

The microstructures and carbon coating effect of the mesoporous $LiFe_{0.6}Mn_{0.4}PO_4$/C microspheres were also carefully examined by SEM and TEM (Fig. 4). The cross-sectional images of a single $LiFe_{0.6}Mn_{0.4}PO_4$/C microsphere from Fig. 4(a) and (b) show that the microspheres are composed of primary particles with a size less than 100 nm. Interconnected mesopores and MWCNTs exist among the primary particles. The existence of the mesopores in the microspheres or on the surface of the microspheres is good for infiltration of liquid electrolyte and increases the transportation rate of the Li^+ in the microspheres. The cross sectional SEM–EDX spectra and the elemental mapping images of the as-synthesized $LiFe_{0.6}Mn_{0.4}PO_4$/C with 2% MWCNTs further confirm the existence and uniform distribution of C, O, P, Fe, and Mn elements among the interior of the microspheres (Supporting information Fig. S1). Specifically, we can observe that the carbonous material distribute uniformly along with the cross section (Fig. S1(d)), and wrapped with other elements inside the particle to work as an interconnected conductive network, which clearly demonstrated in Fig. S1(c). Also, from Fig. 4(c), we can figure out that the size of the primary particles is about 50–100 nm with thin amorphous carbon film coated on the surface. Relatively dark districts are $LiFe_{0.6}Mn_{0.4}PO_4$ crystal, and the relatively grey districts are amorphous carbon. The cross-sectional HRTEM image in Fig. 4(d) supplementary verifies the highly ordered crystalline structure of the $LiFe_{0.6}Mn_{0.4}PO_4$/C microspheres. Accordingly, the crystallinity of the as-synthesized products is well developed and the thickness of the carbon layer is about 3 nm. These surface coated carbon layers and entangled MWCNTs in the microspheres together construct the interconnected conducting network of the microspheres, increasing the discharge capability at elevated current.

Samples of mesoporous $LiFe_{0.6}Mn_{0.4}PO_4$/C microspheres were further investigated by Raman spectroscopic analysis, aiming to confirm the existence of MWCNTs as shown in Fig. 5. Similar peak shapes and positions in the Raman spectroscopy are noted in the composites. The mode at 945 cm^{-1} is related to the stretching vibration of PO_4^{3-}, while the modes at 1339 cm^{-1} and 1596 cm^{-1} correspond to the D (sp3) and G band (sp2) of carbon materials respectively [34]. Generally, the D band is due to the structural defects and amorphous carbon particles that adsorbed on the walls of MWCNTs, reflecting the defect and disorder in the MWCNTs, while the G band is due to the E_{2g} vibration mode of graphite plane, reflecting the degree of order. The integrated intensity ratio I_D/I_G is an indication of the degree of graphitization, which gives the information of the relative amount and purity of the MWCNTs in the products. The smaller the ratio is, the larger relative amount of MWCNTs exists in the products [35]. From Fig. 5, we know that with

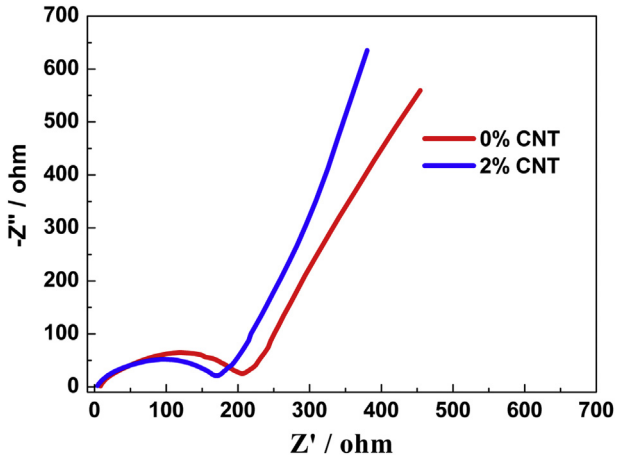

Fig. 12. Nyquist plots of $LiFe_{0.6}Mn_{0.4}PO_4$/C microspheres without and with 2% MWCNTs.

the increase of the MWCNTs addition, the integral area and intensity of the G band enhance gradually. The integral G band area of the $LiFe_{0.6}Mn_{0.4}PO_4$/C composite without MWCNTs is 18.91%. However, that of the $LiFe_{0.6}Mn_{0.4}PO_4$/C composite with 3% MWCNTs embedded is 30.84%. The increase of the G band integral area indicates that the graphitization degree of carbon in the mesoporous $LiFe_{0.6}Mn_{0.4}PO_4$/C microspheres rises with the addition of the MWCNTs, which can further improve the electronic conductivity.

XPS of the mesoporous $LiFe_{0.6}Mn_{0.4}PO_4$/C microspheres with different MWCNTs content was also examined (Fig. 6). The C1s peak can be decomposed to three distinct peaks at the positions of 284.68 eV, 285.31 eV, and 288.6 eV. Among these peaks, 284.68 eV is related to the graphite plane, which is sp2 carbon property; 285.31 eV is linked with the sp3 carbon; and 288.6 eV is ascribed to oxygen-containing groups [36]. According to these images, with the increase of the addition amount of MWCNTs, the integral area of the sp2 C peaks (284.68 eV) escalates gradually (from 32.58%, 42.56%, 42.65%, to 53.28%), while the integral area of the sp3 C peaks decreases gradually (from 47.78%, 32.31%, 31.12%, to 29.49%). Above all, the XPS analysis results are consistent with the Raman spectroscopy, which means that the addition of the MWCNTs can enhance the content of the graphitic carbon in the mesoporous $LiFe_{0.6}Mn_{0.4}PO_4$/C microspheres.

The N_2 adsorption–desorption isotherm and BJH pore size distribution were presented in Fig. 7. The $LiFe_{0.6}Mn_{0.4}PO_4$/C microspheres exhibit a BET surface area of 22.36 $m^2\ g^{-1}$ and a mainly pore size distribution of 35 nm. The formation of these pores might be attributed to the decomposition or partial oxidation of sucrose combined with spray drying process. With a melting point of 186 °C, sucrose undergoes a process of melting, polymerization decomposition, and carbonization at a higher temperature, generating gas products such as CO_2 and CO, which are responsible for the formation of pores in the $LiFe_{0.6}Mn_{0.4}PO_4$/C microspheres. These interconnected mesopores can enhance the infiltration of the electrolyte to the electrode materials, thus improving the electrochemical performance.

With pure olivine-structure phase and interconnected conducting network, the composites exhibit excellent electrochemical properties, which were systematically evaluated in coin cells as shown in Fig. 8. In the view of comprehensive performance or keeping balance between discharge capacity and rate capability, 2 wt% MWCNTs addition was assessed as the optimized condition. Cells were charged at 0.1 C to 4.5 V and discharged at different rates to 2.0 V. Fig. 8(a) and (b) gives the information of the rate performance of bare $LiFe_{0.6}Mn_{0.4}PO_4$/C microspheres without MWCNTs. Discharge capacity of bare $LiFe_{0.6}Mn_{0.4}PO_4$/C microspheres at 0.1 C is 160.2 mAh g^{-1}. With the increase of the current density, the discharge capacities reduce slowly, which are 149.82, 146.20, 139.25, 133.97, 123.30, and 106.27 mAh g^{-1} at 0.5 C, 1.0 C, 3.0 C, 5.0 C, 10 C, 20 C, respectively. However, when the current density is raised to 50 C, the voltage fades to 2.0 V quickly, with a capacity of only 12.8 mAh g^{-1}. In contrast, $LiFe_{0.6}Mn_{0.4}PO_4$/C microspheres with 2% MWCNTs show obviously improved discharge capability at elevated C-rates. The discharge capacities of $LiFe_{0.6}Mn_{0.4}PO_4$/C microspheres with 2% MWCNTs are 163.3, 153.7, 148.7, 137.3, 131.0, 120.9, and 114.4 mAh g^{-1} at 0.1 C, 0.5 C, 1.0 C, 3.0 C, 5.0 C, 10 C, and 20 C, respectively. Even when the current density is increased to 50 C, $LiFe_{0.6}Mn_{0.4}PO_4$/C microspheres with 2% MWCNTs can still deliver a capacity of 64.23 mAh g^{-1} and a discharge voltage plateau at 2.5 V. In addition, the discharge profile of the MWCNTs embedded sample shows more slop and shorter plateau than the control sample of $LiFe_{0.6}Mn_{0.4}PO_4$/C. This may be due to pseudocapacitance brought about by MWCNTs, but the exact reason is still under investigation. The similar phenomenon has also been observed and discussed in graphene supported $LiFePO_4$ [37]. The results indicate that although the addition of MWCNTs has a limited improvement on discharge capacity at low rate, it can generate an obvious improvement on the discharge performance at high rates.

Working as conductive fillers to construct conductive percolation network, small CNT mass loadings can be essential to compensate for a comparable conductivity in a composite. Therefore, the use of CNTs could achieve much better improvement on the electrical conduction compared to conventional carbon additives due to a sufficiently interconnected conductive network. Furthermore, as a result of the nature of p-orbital overlap, the electron conduction can occur via ballistic transport (electrons transfer with mean free paths along the length of the nanotube), which has the potential for increased C-rate performance at high current when used as an additive, especially when combined with the poor transport inherent to cathode materials [38]. According to the relative references, the improvement of the capacity of $LiFePO_4$/C at low rate mainly depends on the surface conductivity of the particles, while the discharge capability at high rates heavily depends on the fast transference of electrons in the interconnected network between particles [28,29]. In the case of $LiFe_{0.6}Mn_{0.4}PO_4$/C microspheres without MWCNTs, although amorphous carbon firmly coated on the surface of particles, the poor conductivity of the amorphous carbon and lack of conducting network make the electrons transport only at a small rate while electron transportation at high rates is much limited (as showed in Fig. 9(a)). However, with the MWCNTs embedded, entangled conducting network establishes in the microspheres and it is good for fast charge transfer at high rates (as showed in Fig. 9(b)). This is also consistent with the rate performance of $LiFe_{0.6}Mn_{0.4}PO_4$/C microspheres in Fig. 8. As a cathode with both high energy density and high power density, the MWCNTs loaded $LiFe_{0.6}Mn_{0.4}PO_4$/C microspheres are promising for the large scale applications such as electric vehicles requiring more safety, higher power density, higher energy density and longer life.

Cycling performance of $LiFe_{0.6}Mn_{0.4}PO_4$/C microspheres without and with 2% MWCNTs was further investigated at room temperature and high temperature (Fig. 10). At 25 °C, the $LiFe_{0.6}Mn_{0.4}PO_4$/C microspheres without MWCNTs exhibit stable cycling performance with capacity of 149, 139, and 124 mAh g^{-1} after 200 cycles at 0.5 C, 1.0 C, and 5.0 C. At high temperature (45 °C), they still deliver stable cycle capacity of 155 mAh g^{-1} at 1.0 C after 300 cycles and 133 mAh g^{-1} at 5.0 C after another 200 cycles. Comparatively, the

microspheres with 2% MWCNTs also deliver sustainable cycling capacity of 150, 145, and 125 mAh g^{-1} after 200 cycles at 0.5 C, 1.0 C, and 5.0 C, respectively. Moreover, the microspheres exhibit stable cycle capacity of 158 mAh g^{-1} at 1.0 C after 300 cycles and 145 mAh g^{-1} at 5.0 C after another 200 cycles at high temperature (45 °C). What's more, the mid-voltages are quite stable during the cycles. Capacity fading can only be observed during the first several cycles, and cycling data becomes relatively stable in the subsequent cycles both at 45 °C and 25 °C for the two samples. The discharge capacity loss during the first several cycles is actually ascribed to increase of current density after former cycles at low current (0.1 C). Generally, elevated temperature can accelerate the manganese dissolution and electrolyte decomposition, leading to serious discharge capacity fading and plateau decay during prolonged cycle process. However, the firmly surface-coated carbon layer and intertwined MWCNTs could protect the electrode from failure and alleviate the manganese dissolution and electrolyte decomposition. What's more, lithium ion and electron diffusion rates are also enhanced at high temperature [39]. Therefore, the as-prepared microspheres can still have even better electrical performance at high temperature.

CV tests of the as-prepared $LiFe_{0.6}Mn_{0.4}PO_4/C$ microspheres without and with 2% MWCNTs were carried out in a voltage range of 2.0–4.5 V vs. Li^+/Li (Fig. 11). It is clear that both of the samples exhibit two pair of anodic and cathodic peaks at 3.5 V and 4.1 V, corresponding to the Fe^{2+}/Fe^{3+} and Mn^{2+}/Mn^{3+} redox process. Within sequential CV tests at different scan rates of 0.05, 0.1, 0.3, 1.0 mV s^{-1} as shown in Fig. 11(a) and (c), the potential differences between the pair of redox peaks have enlarged with the increased scan rates, but the small variation reflects good reversibility of the electrodes, which could be ascribed to the rapid ion-exchange. What's more, it is noticed that there is a good linear relationship between the peak current (I_p) and the square root of scan rate $v^{1/2}$ (Fig. 11(b) and (d)), illustrating a diffusion-controlled process for the whole electrode reaction. Thus, the ion diffusion is a key factor to the electrode kinetics. Accordingly, the Li^+ diffusion coefficient Ds can be calculated (Fig. 11(e)). From Fig. 11(e), we can notice that the $LiFe_{0.6}Mn_{0.4}PO_4/C$ microspheres with 2% MWCNTs exhibit larger Ds than that of the bare sample, which can provide further evidence for the importance of MWCNTs existed in the samples.

Electrochemical Impedance Spectroscopy (EIS) measurements were also performed on the $LiFe_{0.6}Mn_{0.4}PO_4/C$ micro-spherical electrodes after 3 cycles to provide more information for the improved electrochemical performance (Fig. 12). The spectra of the samples have similar profiles which are composed of a semicircle in the high-to-medium frequency region and an inclined line in the low frequency region. The semicircle is approximately ascribed to the charge transfer process, and the inclined line is associated with the long-range Li^+ diffusion [40]. Apparently, with a smaller semicircle, the $LiFe_{0.6}Mn_{0.4}PO_4/C$ microspheres with 2% MWCNTs exhibit a smaller charge transfer resistance than the bare sample due to the addition of MWCNTs and the interconnected network constructed in the microspheres.

4. Conclusions

In this work, a series of $LiFe_{0.6}Mn_{0.4}PO_4/C$ composites with different amount of MWCNTs was fabricated successfully by introducing MWCNTs to $LiFe_{0.6}Mn_{0.4}PO_4$ during the spray drying process. MWCNTs can entangle with the primary particles to construct conductive network in the microspheres, which facilitates fast charge transfer of the electrode. The as-prepared materials show improved electrochemical performance especially at high rates. Therefore, the $LiFe_{0.6}Mn_{0.4}PO_4/C$ microspheres with 2% MWCNTs can still deliver capacity of 64.23 mAh g^{-1} at 50 C, while that of bare $LiFe_{0.6}Mn_{0.4}PO_4/C$ is only 12.8 mAh g^{-1}, which demonstrates that the addition of MWCNTs can largely improve the discharge ability at high current density. What's more, the MWCNTs loaded microspheres show no obvious capacity fades or voltage decay after 500 cycles at 45 °C. With high safety property, superior power density, high energy density and high stability, the MWCNTs loaded $LiFe_{0.6}Mn_{0.4}PO_4/C$ microspheres are very promising for the next generation lithium ion batteries in large scale applications as electric vehicle and grid energy storage. The fabrication method used here is cheap, facile and scalable, which can also offer a way to improve the rate capability of other materials with limitation of sluggish conductivity or low tap density.

Acknowledgements

A*Star Singapore–China Joint Research program (No. 2012DFG52130) and Pulead Technology Industry Co. Ltd are gratefully acknowledged for their financial support for this work.

Appendix A. Supplementary data

Supplementary data related to this article can be found at http://dx.doi.org/10.1016/j.jpowsour.2014.05.102.

References

[1] A.K. Padhi, K.S. Nanjundaswamy, J.B. Goodenough, J. Electrochem. Soc. 144 (1997) 1188–1194.
[2] J.F. Qian, M. Zhou, Y.L. Cao, X.P. Ai, H.X. Yang, J. Phys. Chem. C 114 (2010) 3477–3482.
[3] C. Sun, S. Rajasekhara, J.B. Goodenough, F. Zhou, J. Am. Chem. Soc. 133 (2011) 2132–2135.
[4] G. Wang, H. Liu, J. Liu, S. Qiao, G.M. Lu, P. Munroe, H. Ahn, Adv. Mater. 22 (2010) 4944–4948.
[5] M.-H. Lee, J.-Y. Kim, H.-K. Song, Chem. Commun. 46 (2010) 6795–6797.
[6] Y. Wang, Y. Wang, E. Hosono, K. Wang, H. Zhou, Angew. Chem. Int. Ed. 47 (2008) 7461–7465.
[7] N. Ravet, J. Power Sources 97-98 (2001) 503–507.
[8] Y.-H. Huang, J.B. Goodenough, Chem. Mater. 20 (2008) 7237–7241.
[9] Y.S. Hu, Y.G. Guo, R. Dominko, M. Gaberscek, J. Jamnik, J. Maier, Adv. Mater. 19 (2007) 1963–1966.
[10] Y.D. Li, J. Alloys Compd. 509 (2011) 957–960.
[11] S.-Y. Chung, J.T. Bloking, Y.-M. Chiang, Nat. Mater. 1 (2002) 123–128.
[12] N. Meethong, Adv. Funct. Mater. 19 (2009) 1060–1070.
[13] C. Ban, W.J. Yin, H. Tang, S.H. Wei, Y. Yan, A.C. Dillon, Adv. Energy Mater. 2 (2012) 1028–1032.
[14] L.-e. Li, J. Liu, L. Chen, H. Xu, J. Yang, Y. Qian, RSC Adv. 3 (2013) 6847–6852.
[15] V. Aravindan, J. Gnanaraj, Y.-S. Lee, S. Madhavi, J. Mater. Chem. A 1 (2013) 3518–3539.
[16] W. Liu, P. Gao, Y. Mi, J. Chen, H. Zhou, X. Zhang, J. Mater. Chem. A 1 (2013) 2411–2417.
[17] Z.-Q. Huo, Y.-T. Cui, D. Wang, Y. Dong, L. Chen, J. Power Sources 245 (2014) 331–336.
[18] J. Hong, J. Power Sources 196 (2011) 3659–3663.
[19] D. Bhuvaneswari, Gangulibabu, C.-H. Doh, N. Kalaiselvi, Int. J. Electrochem. Sci. 6 (2011) 3714–3728.
[20] A. Yamada, Y. Kudo, K.-Y. Liu, J. Electrochem. Soc. 148 (2001) A747–A754.
[21] J. Molenda, W. Ojczyk, J. Marzec, J. Power Sources 174 (2007) 689–694.
[22] T. Muraliganth, A. Manthiram, J. Phys. Chem. C 114 (2010) 15530–15540.
[23] G. Li, H. Azuma, M. Tohda, J. Electrochem. Soc. 149 (2002) A743–A747.
[24] M.R. Roberts, G. Vitins, G. Denuault, J.R. Owen, J. Electrochem. Soc. 157 (2010) A381–A386.
[25] C. Li, N. Hua, C. Wang, X. Kang, T. Wumair, Y. Han, J. Alloys Compd. 509 (2011) 1897–1900.
[26] Y.K. Sun, S.M. Oh, H.K. Park, B. Scrosati, Adv. Mater. 23 (2011) 5050–5054.
[27] J. Xu, G. Chen, X. Li, Mater. Chem. Phys. 118 (2009) 9–11.
[28] J. Wang, X. Sun, Energy Environ. Sci. 5 (2012) 5163–5185.
[29] I.V. Thorat, T. Joshi, K. Zaghib, J.N. Harb, D.R. Wheeler, J. Electrochem. Soc. 158 (2011) A1185–A1193.
[30] X.-M. Liu, B. Zhang, P.-C. Ma, M.M. Yuen, J.-K. Kim, Compos. Sci. Technol. 72 (2012) 121–144.
[31] P.G. Bruce, B. Scrosati, J.-M. Tarascon, Angew. Chem. Int. Ed. 47 (2008) 2930–2946.
[32] J. Chen, M.S. Whittingham, Electrochem. Commun. 8 (2006) 855–858.

[33] L. Wang, Y. Huang, R. Jiang, D. Jia, J. Electrochem. Soc. 154 (2007) A1015–A1019.
[34] K. Sheem, Y.H. Lee, H.S. Lim, J. Power Sources 158 (2006) 1425–1430.
[35] M.S. Dresselhaus, G. Dresselhaus, R. Saito, A. Jorio, Phys. Rep. 409 (2005) 47–99.
[36] S. Yoon, C. Liao, X.-G. Sun, C.A. Bridges, R.R. Unocic, J. Nanda, S. Dai, M.P. Paranthaman, J. Mater. Chem. 22 (2012) 4611–4614.
[37] Y. Wang, D. Zhao, R. Che, Y. Xia, J. Power Sources 236 (2013) 230–237.
[38] B.J. Landi, M.J. Ganter, C.D. Cress, R.A. DiLeo, R.P. Raffaelle, Energy Environ. Sci. 2 (2009) 638–654.
[39] X.-L. Pan, C.-Y. Xu, D. Hong, H.-T. Fang, L. Zhen, Electrochim. Acta 87 (2013) 303–308.
[40] S. Liu, H. Fang, B. Yang, Y. Yao, W. Ma, Y. Dai, J. Power Sources 230 (2013) 267–270.